

# Integrating S/TEM Imaging Modality Simulations with Mesoscale Material Simulations: A Case Study with Phase Field

Saransh Singh<sup>1</sup>, Marc De Graef<sup>1</sup>

<sup>1</sup> Dept. of Materials Science and Engineering, Carnegie Mellon Univ., Pittsburgh PA 15213, USA

Defect image contrast simulations for TEM modalities have a long tradition and have played a crucial role in interpreting contrast features observed in electron micrographs. The development of the dynamical diffraction theory for electrons led to a number of early computer programs for performing such simulations. Initially, hardware limitations allowed only for solution of the two beam case, and then only for special geometries. However, with the improvement in the computer hardware, system-atic row, zone-axis and general  $n$ -beam simulations are now routinely performed. While the current programs are able to handle more general diffraction conditions, the simulations still require analytical displacement fields to describe the defects. This severely limits the capability to perform simulations for complex defect configurations which are present in many engineering materials. Therefore, there is a pressing need to augment the existing framework and incorporate defect image simulations for more realistic cases. In this contribution, we discuss an extension of the existing defect simulation framework to include mesoscale material simulation techniques, namely phase field (PF) simulations; the approach should also be able to handle the output from discrete dislocation dynamics simulations (DDD). In addition to these two mesoscale simulation techniques, the dynamical scattering framework is also extended to account for the special case of coherent two-phase systems such as the technologically relevant Ni/Co based superalloys. Furthermore, simulation strategies for both parallel and converged probe illumination are discussed.

The well known Darwin-Howie-Whelan (DHW) system of equations can be used to describe the scattering of electrons by crystals. The DHW equations describe how the probability amplitude of an electron wave changes as a function of depth in a crystal. The probability amplitudes are governed by the diffraction geometry as well as the interaction strength of the various beams. In the presence of defects, atoms are displaced from their lattice positions which results in broken translational symmetry. In the presence of a displacement field,  $\mathbf{R}(\mathbf{r})$ , the DHW equations are modified and are given by the following first order coupled partial differential equation

$$\frac{d\psi_{\mathbf{g}}}{dz} = 2\pi i s_{\mathbf{g}} \psi_{\mathbf{g}} + i\pi \sum_{\mathbf{g}' \neq \mathbf{g}} \frac{e^{i\theta_{\mathbf{g}} - \theta_{\mathbf{g}'}}}{q_{\mathbf{g} - \mathbf{g}'}} e^{i\alpha_{\mathbf{g} - \mathbf{g}'}} \psi_{\mathbf{g}'}, \quad (1)$$

where,  $\psi_{\mathbf{g}}$  is the probability amplitude for the reciprocal reflection  $\mathbf{g}$ ,  $s_{\mathbf{g}}$  is the excitation error which depends on the diffraction geometry,  $q_{\mathbf{g}}$  is the interaction strength and  $\alpha_{\mathbf{g}} \equiv 2\pi \mathbf{g} \cdot \mathbf{R}(\mathbf{r})$ . The displacement field,  $\mathbf{R}(\mathbf{r})$  is typically computed using analytical expressions; e.g., for straight dislocations, the displacement fields are calculated using linear elasticity theory. The equations are commonly written in matrix form, and broken up as a Hadamard product (denoted by  $\circ$ ) of two matrices, a matrix for the perfect crystal and a defect matrix, with a formal solution given by the exponential of a matrix. These equations are shown collectively as:

$$\frac{d\Psi}{dz} = i\mathcal{A}\Psi; \quad \mathcal{A}_{\mathbf{g}\mathbf{g}'} = \begin{cases} 2\pi s_{\mathbf{g}} & : \mathbf{g} = \mathbf{g}' \\ \frac{e^{i\theta_{\mathbf{g}} - \theta_{\mathbf{g}'}}}{q_{\mathbf{g} - \mathbf{g}'}} e^{i\alpha_{\mathbf{g} - \mathbf{g}'}} & : \mathbf{g} \neq \mathbf{g}' \end{cases}; \quad \mathcal{A}^d(\mathbf{r}) = \mathcal{A}^p(\mathbf{r}) \circ V^d(\mathbf{r}); \quad \Psi(z) = e^{i\mathcal{A}z} \Psi(0)$$

In the presence of a coherent second phase, the expression for  $\mathcal{A}$  in the above equation is modified. For the case of the coherent primitive L1<sub>2</sub>  $\gamma'$  phase in the fcc  $\gamma$  matrix with 4 translational variants, the structure matrix is given by the following expression:

$$\mathcal{A}^{\text{eff}}(\mathbf{r}) = \left[ f_{\gamma}(\mathbf{r})\mathcal{A}_{\gamma}^p + \sum_{\alpha=1}^4 f_{\gamma'}^{\alpha}(\mathbf{r})\mathcal{A}_{\gamma'}^p \circ V^{\alpha}(\mathbf{r}) \right] \circ V^d(\mathbf{r}).$$

Here,  $f_{\gamma}(\mathbf{r})$  and  $f_{\gamma'}^{\alpha}(\mathbf{r})$  are the order parameters in the phase field simulation for the matrix and the translational variants and  $V^{\alpha}(\mathbf{r})$  is the phase shift due to lattice translation with respect to the matrix. Due to the primitive nature of the  $\gamma'$  phase all reflections are allowed whereas there are systematic absences in the lattice centered  $\gamma$  phase. However, the equations reveal that the superlattice reflections in the  $\gamma$  phase can attain non-zero amplitude and propagate through the disordered matrix. Furthermore, these superlattice reflections are fully decoupled from the fundamental reflections.

In the STEM mode, the coherent converged probe is decomposed into a sum of plane waves with slightly different wavevectors such that the overall scattering is a sum of scattering for the different wave vectors. It is important to note that for small convergence angles, changes in the wave vector only affect the off-diagonal component of the structure matrix. This can be used to design efficient simulations strategies for the case of a converged probe.

Fig. 1(a) shows the initial phase field microstructure in a Ni-Al superalloy, with different colors showing different translational variants of the  $\gamma'$  phase. The empty space corresponds to the  $\gamma$  matrix. Fig. 1(b) shows the bright/dark field images in the parallel illumination mode at their respective location in the (001) zone axis.

### References:

- [1] S. Singh, M.J. Mills, M. De Graef, *Ultramicroscopy*, **185**, 32-41, 2018.  
 [2] The authors acknowledge R. Shi (LLNL) for providing the phase field data set, an ONR Vannevar Bush Faculty Fellowship (N00014-16-1-2821), and the computational resources of the Materials Characterization Facility at CMU, grant MCF-677785.

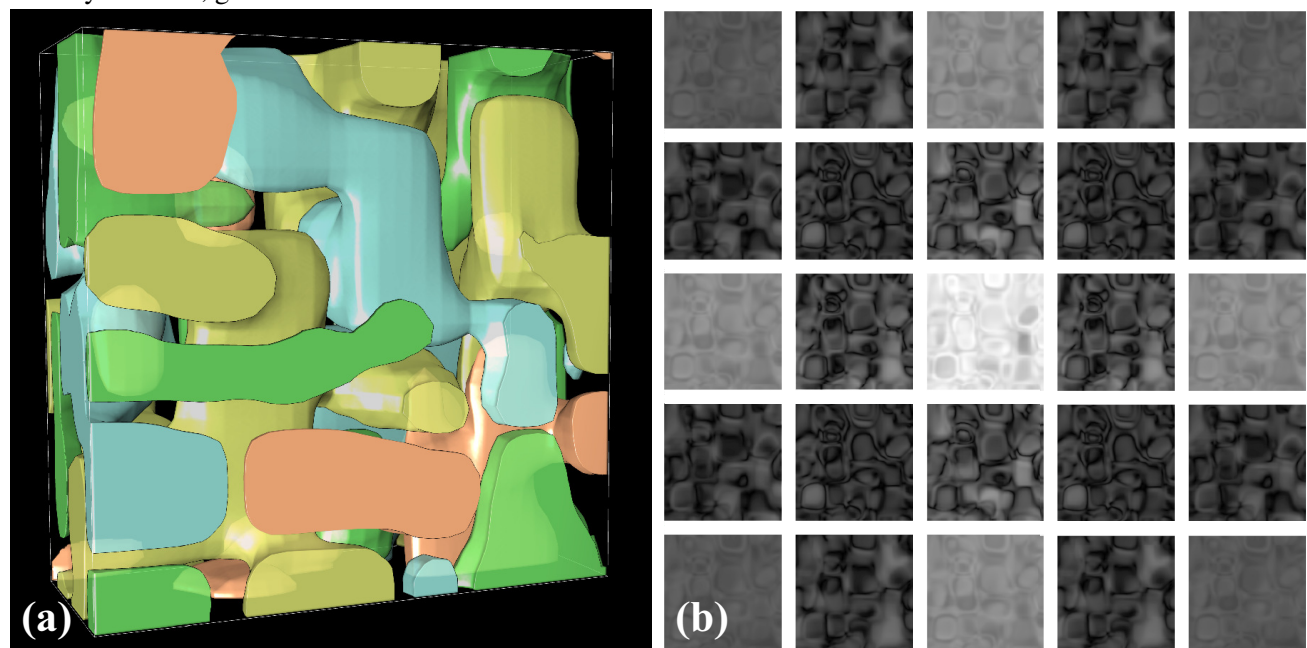


**Figure 1.** (a) Phase field microstructure and (b) Bright and dark field images.